

Verification of model wave heights with long-term moored buoy data: application to wave field over the Indian Ocean

V. Samiksha¹, V.G. Polnikov², P. Vethamony^{1*}, R. Rashmi¹, F. Pogarskii² and K. Sudheesh¹

¹CSIR-National Institute of Oceanography, Dona Paula, Goa - 403004, India

²Obukhov Inst. for Phy. of the Atmosphere, Russian Academy of Sciences, Moscow, Russia.

* Corresponding author: P. Vethamony, Chief Scientist, Physical Oceanography Division, ¹National Institute of Oceanography, Dona Paula, Goa – 403004, India. Email: mony@nio.org. Tel.: +91 832 2450473. Fax.: +91 832 2450608.

V. Samiksha: vsamiksha@nio.org

V.G. Polnikov: polnikov@mail.ru

R. Rashmi: rrashmi@nio.org

F. Pogarskii: soimynailmene@rambler.ru

K. Sudheesh: sudheesh@nio.org

Abstract

This paper describes the results obtained using a modified version (ModWAM) of the global wave model WAM, in which new parameterizations have been applied based on the seasonal changes and extreme weather events that have occurred in the Indian Ocean. Model significant wave heights (H_s) have been verified using H_s data extracted for the period 2000-2006 from 10 moored data buoys, deployed in the north Indian Ocean. Satellite altimeter H_s have also been used for the model comparison. Based on the error estimates of significant wave heights and spectral wave energy, improvement achieved in wave prediction using ModWAM is demonstrated. We find that the ModWAM improved the accuracy of significant wave height prediction in deep water considerably (rmse of ModWAM is less than that of rmse of WAM), and provided better presentation for high waves that prevailed during southwest monsoon (e.g. H_s , of the order of. 6.0 m in June 2005) and extreme weather events (e.g. cyclone that occurred in May 2005), compared to WAM; but, it still underestimates H_s for high waves. Comparison between modelled and measured spectra shows that ModWAM overpredicts spectral energy at low frequencies, and underpredicts at high frequencies.

Keywords: Wind wave prediction, WAM wave model, Source functions, Moored buoy data, the Indian Ocean, Significant wave height, Error estimates

1. Introduction

Wind waves play crucial roles in marine processes such as exchange of gases, heat and momentum between the atmosphere and the sea, interchange of energy with currents and interaction with bottom. Hence, the requirement for high quality wave data is constantly increasing not only in the areas of offshore oil exploration, marine transportation and structural design, but also in fundamental research. In order to study these processes, high resolution spatial and temporal wave data are required, and this is possible only through wave modeling. Hence, the wave modeling community is ever on the task of understanding and applying the physical processes in wave models in order to increase its accuracy and performance. The main approach to accurate prediction of sea state is to use of numerical modeling techniques in conjunction with atmospheric models, data assimilation systems and statistical techniques (WAMDI Group, 1988; Lionello et al., 1992; Komen et al., 1994; Abdalla et al, 2005; Chu and Cheng, 2008, Tolman et al. 2012). The various techniques mentioned in these scientific works have been successful in predicting the sea state reasonably accurately on global as well as regional scales. It may be noted that besides the time required for the calculations, the issue of model accuracy is the most important, since the discrepancies between the results obtained with different models can sometime appear to be too great (Tolman et al., 2002, Cavaleri et al., 2007).

In deep water, the wind input, nonlinear wave-wave interaction and breaking dissipation are the three most important source terms governing the dynamics of the surface gravity wave evolution (for e.g., Hasselmann et al., 1973; Phillips, 1977, 1985; Komen et al., 1994; Janssen, 2004, Violante-Carvalho et al., 2004). The physics of these source functions are still active research subjects, and one of the methods to gauge the performance of numerical or theoretical wave models is to compare the model results with fetch- or duration limited wave growth functions (e.g., Komen et al., 1984, 1994; Janssen et al., 1994; Ardhuin et al., 2007; Romero and Melville, 2010). As ‘duration limited condition’ occurs rarely in the natural environment, by far, research on fetch-limited growth contributes the most to the benchmark database. Over the last few decades, many fetch growth functions have been proposed (e.g., reviews by Hasselmann et al., 1973; Donelan et al., 1985; Kahma and Calkoen, 1994). Kukulka and Hara (2005) proposed a wind input wave growth formulation under the sheltering assumption. According to this approach, the wave-induced stress of longer waves reduces the turbulent stress felt by shorter waves. More recently, Banner and Morison (2010) and Ardhuin et al. (2010) proposed a wave prediction model based on quasi-linear theory, resulting in an effective high wave number cut-off, including slight tuning modifications.

The basic equations for nonlinear interactions were proposed by Hasselmann (1962, 1963a,b) and later modified by Zakharov (1968). Further, a lot of parameterizations for the finite depth version of the interaction coefficient were proposed by Webb (1978), Dungey and Hui (1979), Herterich and Hasselmann (1980) and Zakharov (1999). Gorman (2003) provided a detailed analysis of finite depth interaction coefficient and derived expressions for the treatment of discontinuities. Lavrenov et al., (2001, 2003) gave an efficient numerical algorithm for simulating nonlinear energy transfer using the Hasselmann kinetic equation for gravity waves in water surface. In this approach, the kinetic equation for surface gravity waves was investigated numerically taking into account an external generating force and dissipation. Tolman (2013) proposed a new DIA (Discrete Interaction Approximation) approximation as Generalized Multiple DIA (GMD) for nonlinear four-wave interactions in wind wave spectra. GMD was tested for different scenarios and found that GMD is capable of removing most of the errors introduced by the DIA in deep water. In shallow water the GMD is capable of reproducing shallow water behavior of the exact interactions, albeit with some spurious shifting of energy to lower frequencies in extremely shallow water.

Over the past decade, many physical features of the dissipation performance were carried out experimentally and through field measurements. For example, the threshold behavior of wave breaking (Babanin et al. 2001, 2011; Banner et al. 2002), the cumulative effect of wave dissipation at smaller scales and therefore two-phase behavior of the dissipation (Manasseh et al. 2006; Young and Babanin 2006), quasi-singular behavior of the dissipation in the middle wavelength range (Hwang and Wang 2004). Polnikov (1993) assumed a simplified representation of wave dynamic equations with the efficient stress attenuation that is appropriate for monochromatic waves. Recently, Chalikov and Babanin (2012) studied wave breaking and dissipation by modelling the breaking in spectral environments. Galchenko et al. (2012) carried out laboratory investigation of wave influence on modulational instability, breaking and dissipation.

In most of the present numerical models, the evolution of wind waves is usually written in the form of a wave transport equation for the two-dimensional wave spectrum. From mathematical point of view, a wind wave field has a stochastic feature, and its properties should be governed by a proper statistical ensemble. Therefore, the best way to describe the phenomenon lies in the domain of statistical characteristics. The most significant of them is the two-dimensional spatial wave energy spectrum, $F(k,x,t)=F$, spread in the space, x , and time, t . The space-time evolution is described in the spectral representation (Komen et al., 1984):

$$\frac{\partial F}{\partial t} + C_{gx} \frac{\partial F}{\partial x} + C_{gy} \frac{\partial F}{\partial y} = S = NL + IN - DIS \quad (1)$$

The LHS is the full time-derivative of the spectrum, and the RHS is the source function (“forcing”) term, S . Vector (C_{gx}, C_{gy}) is the group velocity corresponding to a wave component with wave vector \mathbf{k} , which is defined by

$$\mathbf{C}_g = \frac{\partial \sigma(k)}{\partial k} \frac{\mathbf{k}}{k} = (C_{gx}, C_{gy})$$

Dependence of frequency on the wave vector $\sigma(\mathbf{k})$ is given by the expression, $\sigma = \sqrt{gk}$ known as the dispersion relation for the case of deep water. The LHS of eqn (1) is responsible for “mathematical” part of the model, which is not discussed here, whilst the physical essence of the model is held by the source function, S . The total source function S , is modelled as the sum of three terms, which are involved in the combined evolution mechanism for wind waves: (i) the rate of energy transfer from wind to waves, IN (input term), (ii) the rate of conservative non-linear energy transfer through a wave spectrum, NL (non-linear term) and (iii) the rate of wave energy loss due to various dissipative processes, DIS (dissipation term). The different parameterizations used for the source functions define physical processes of each model. In our earlier work, we used wave models to study the wave characteristics (swell-sea interaction, waves generated by shamal winds, storm generated waves and propagation of southern swells in the north Indian Ocean) of the Indian Ocean (Aboobacker et al. 2009, 2011a, 2011b, 2013; Vethamony et al. 2009, 2011; Samiksha et al. 2012; Rashmi et al. 2013). In the present study, we have used the modified model of WAM (Pogarskii et al, 2012; Polnikov et al., 2012, 2013) to study the wind wave variability in the Indian Ocean; the model results were verified with long-term buoy data at several locations in the Indian Ocean.

2. Methodology

The WAM model (Cycle 4) is a third generation wave model, which solves the wave transport equation explicitly without any presumptions on the shape of the wave spectrum (WAMDI group, 1988). It represents physics of the wave evolution in accordance with full set of degrees of freedom of a two dimensional wave spectrum. The model runs for any given regional or global grid system with a prescribed topographic dataset - the grid resolution can be arbitrary in space and time. The propagation can be done on a latitudinal- longitudinal or Cartesian grid.

ModWAM model

ModWAM is a modified version of WAM model. In ModWAM (Polnikov, 2003, 2005, 2012a), the three source functions are modified as follows:

i) The wind-wave energy exchange term, In , is written in the commonly used representation as follows:

$$In = \beta(\sigma, \theta, u_*)\sigma S(\sigma, \theta) \quad (2)$$

In ModWAM, the wave growth increment $\beta(\sigma, \theta, u_*)$ has been modified as

$$\beta = C_{IN} \max\{-b_L, \beta_Y\} \quad (3)$$

where, C_{IN} is the general fitting coefficient, whilst b_L is the auxiliary fitting parameter responsible for negative values of β for waves overtaking the local wind W_{10} taken at the standard height, $z=10$ m. In the model, wind W_{10} is converted to frictional velocity, u_* using the dynamic water boundary layer approach (Janssen, 2004).

The value β_Y is the combined analytical presentation for β , obtained by Yan (1987) in the form

$$\beta_Y = \left[0.04 \left(\frac{u_* \sigma}{g} \right)^2 + 0.00544 \frac{u_* \sigma}{g} + 0.000055 \right] \cos(\theta - \theta_w) - 0.00031 \quad (3.1)$$

σ and θ are the frequency and propagation angle of a wave component, respectively; u_* is the friction velocity, g is the acceleration due to gravity and θ_w is the local wind direction. It may be noted that parameter β in the parameterization can take negative values, when β_Y becomes less than b_L (for waves overtaking the wind). The optimum value of the latter, as the fitting parameter, is found to be

$$b_L = 0.000002$$

Finally, it may be noted that the waves which overtake the local wind (indicated by negative value of β) must supply their energy to the wind (Galchenko et al, 2012).

ii) For representation of the term NL in the source function, we used the Fast version of the Discrete Interaction Approximation (FDIA), which provides high efficiency (Polnikov, 2003). Polnikov and Farina (2002) proposed a version of the fast DIA, which doubles the speed of calculations without loss of accuracy. Polnikov (2003) modified the original version of DIA to reduce the errors but still in this configuration a major problem is that the interactions represent only a small subset (in which 2 of the interacting wave number vectors are equal, rather than the more general case of 4 unequal wave number vectors) of the total interactions contributing to the complete integral. Numerical expression for FDIA method is given in Polnikov (2005).

The theoretical basis for *NI*-mechanism results from the nonlinear feature of the Euler's equations, that is, four-wave kinetic integral (KI) derived by Hasselmann (1962) and subsequently, re-derived in terms of Hamiltonian method by Zakharov (1968, 1974). In the most compact form, KI can be written as

$$\begin{aligned} \partial N(\mathbf{k}_4) / \partial t \equiv NI[N(\mathbf{k}_4)] = & 4\pi \int d\mathbf{k}_1 \int d\mathbf{k}_2 \int d\mathbf{k}_3 M^2(\mathbf{k}_1, \mathbf{k}_2, \mathbf{k}_3, \mathbf{k}_4) \times \\ & \left[N(\mathbf{k}_1)N(\mathbf{k}_2)(N(\mathbf{k}_3) + N(\mathbf{k}_4)) - N(\mathbf{k}_3)N(\mathbf{k}_4)(N(\mathbf{k}_1) + N(\mathbf{k}_2)) \right] \times \\ & \times \delta[\sigma(k_1) + \sigma(k_2) - \sigma(k_3) - \sigma(k_4)] \delta(\mathbf{k}_1 + \mathbf{k}_2 - \mathbf{k}_3 - \mathbf{k}_4) \end{aligned} \quad (4)$$

Where, $N(\mathbf{k}) = 4\pi^2 g F(\mathbf{k}) \sigma$ is the wave action spectrum (introduced in the Hamiltonian method as the most convenient spectral variable), \mathbf{k}_i is the wave vector corresponding to the frequency-angular wave component (σ_i, θ_i) , ($i = 1, 2, 3, 4$), $M(\dots)$ are the matrix elements describing intensity of interactions between four waves and $\delta(\dots)$ is the Dirac's delta-function providing the resonance feature of the four-wave interactions.

The problem of DIA is that it has several built-in limitations (Cavaleri et al., 2007). The use of exact resonance configuration in the original DIA is not optimal. This configuration is given by the following ratios

$$\mathbf{k}_1 = \mathbf{k}_2 = \mathbf{k}, \text{ where the arbitrary wave vector } \mathbf{k} \text{ is represented by } \sigma \text{ and } \theta; \quad (4.1a)$$

$$\mathbf{k}_3 = \mathbf{k}_+, \text{ where } \mathbf{k}_+ \text{ is represented by } \sigma_+ = \sigma(1 + \lambda) \text{ and } \theta_+ = \theta + \Delta\theta_+; \quad (4.1b)$$

$$\mathbf{k}_4 = \mathbf{k}_-, \text{ where } \mathbf{k}_- \text{ is represented by } \sigma_- = \sigma(1 - \lambda) \text{ and } \theta_- = \theta - \Delta\theta_-; \quad (4.1c)$$

and parameters of the configuration are

$$\lambda = 0.25, \quad \Delta\theta_+ = 11.5^\circ, \quad \Delta\theta_- = 33.6^\circ. \quad (4.1d)$$

The relation between the parameters in 4.1d is governed by the resonant feature of KI (Polnikov, 2003). In such a case, the nonlinear term $NI(\mathbf{k})$ at all \mathbf{k} -points takes the form

$$NI(\mathbf{k}_-) = I(\mathbf{k}, \mathbf{k}_+, \mathbf{k}_-), \quad NI(\mathbf{k}_+) = I(\mathbf{k}, \mathbf{k}_+, \mathbf{k}_-), \quad NI(\mathbf{k}) = -2I(\mathbf{k}, \mathbf{k}_+, \mathbf{k}_-) \quad (4.2)$$

Where,

$$I(\mathbf{k}, \mathbf{k}_+, \mathbf{k}_-) = C_{NL} g^{-8} \sigma^{19} \left[N^2(\mathbf{k})(N(\mathbf{k}_+) + N(\mathbf{k}_-)) - 2N(\mathbf{k})N(\mathbf{k}_+)N(\mathbf{k}_-) \right]. \quad (4.3)$$

where, C_{NL} is the fitting constant for the *NI*-term.

The typical calculations of frequency-angle grid $\{\sigma, \theta\}$ for wave models are given below:

$$\sigma(i) = \sigma_0 \cdot e^{i-1} \quad (0 \leq i \leq I) \quad (5)$$

$$\theta(j) = -\pi + j \cdot \Delta\theta \quad (0 \leq j \leq J) \quad (6)$$

Where, σ_0 is the lowest frequency, e is the exponential increment of the frequency grid, I is the number of frequencies considered, $\Delta\theta = 2\pi/J$ is the angular resolution in radians and J is the number of directions considered. In the present work, we used the same values of these parameters, which are typical of WAM (Cycle 4):

$$\sigma_0 = 2\pi \cdot 0.05 \text{ p/c}; \quad e = 1.1; \quad I = 30; \quad J = 24; \quad \Delta\theta = \pi/12 \quad (7)$$

In such a case, the optimal configuration of the four interacting waves in the version with FDIA is given by the following ratios:

a) for frequencies

$$\sigma_1 = \sigma e^3, \quad \sigma_2 = \sigma e^3, \quad \sigma_3 = \sigma e^5, \quad (8a)$$

b) for angles

$$\theta_1 = \theta + 2\Delta\theta, \quad \theta_2 = \theta + 2\Delta\theta, \quad \theta_3 = \theta + 3\Delta\theta \quad (8b)$$

For known values of σ and θ , the calculating loop is arranged; in this loop, the expression for the term $NL[F(\sigma, \theta)]$ is calculated by the known formulae

$$NL(\sigma, \theta) = I(\sigma_1, \theta_1, \sigma_2, \theta_2, \sigma_3, \theta_3, \sigma, \theta) \quad (9a)$$

$$NL(\sigma_3, \theta_3) = I(\sigma_1, \theta_1, \sigma_2, \theta_2, \sigma_3, \theta_3, \sigma, \theta) \quad (9b)$$

$$NL(\sigma_1, \theta_1) = -I(\sigma_1, \theta_1, \sigma_2, \theta_2, \sigma_3, \theta_3, \sigma, \theta) \quad (9c)$$

$$NL(\sigma_2, \theta_2) = -I(\sigma_1, \theta_1, \sigma_2, \theta_2, \sigma_3, \theta_3, \sigma, \theta) \quad (9d)$$

Where,

$$\begin{aligned} I(\sigma_1, \theta_1, \sigma_2, \theta_2, \sigma_3, \theta_3, \sigma, \theta) = \\ = C\sigma^{Jl} [F_1 F_2 (F_3 + (\sigma_3/\sigma)^4 F) - F_3 F ((\sigma_2/\sigma)^4 F_1 + (\sigma_1/\sigma)^4 F_2)] \end{aligned} \quad (10)$$

In eqns (9) and (10), short notations are used; $F_i = F(\sigma_i, \theta_i)$; index 4 is ignored. Values (σ_i, θ_i) for indices $i = 1, 2, 3$ are given by the relations in eqn. 8. The adjusting constant C has the value of 12000 for optimized version of FDIA in the source function (given above).

iii) The term, *Dis* (Polnikov, 2012a) is represented by the original theoretically substantiated parameterization of the form

$$Dis(\sigma, \theta, F, W) = \tilde{\gamma}(\sigma, \theta, W) \frac{\sigma^4}{g} F^2(\sigma, \theta) \quad (11)$$

Where, the non-dimensional function $\tilde{\gamma}(\sigma, \theta, W)$ is specified as

$$\tilde{\gamma}(\sigma, \theta, W) = c(\sigma, \theta, \sigma_p) \max[0.00005, \beta(\sigma, \theta, u_*)]. \quad (12)$$

The value of $\beta(\sigma, \theta, u_*)$ is defined by eqn (3.1). The non-dimensional function $c(\sigma, \theta, \sigma_p)$ describing the details of dissipation processes in the peak frequency of the spectrum, σ_p is specified as,

$$c(\sigma, \theta, \sigma_p) = C_{dis} \max[0, (\sigma - c_\sigma \sigma_p) / \sigma] T(\sigma, \theta, \sigma_p) \quad (13)$$

with the proposed angular function

$$T(\sigma, \theta, \sigma_p) = \left\{ 1 + 4 \frac{\sigma}{\sigma_p} \sin^2 \left(\frac{\theta - \theta_w}{2} \right) \right\} \max[1, 1 - \cos(\theta - \theta_w)] \quad (14)$$

The factor within the brackets of eqn. 13 plays the role of modulation for the dissipation rate in the spectral peak, and it is responsible for spectral shape. This feature of the *Dis*-term parameterization reflects, to some extent, the cumulative effect proposed in Young and Babanin (2006). It is important to note that the regulator of this effect is the fitting coefficient c_σ , given in small brackets of equation (13). Coefficient C_{dis} regulates the intensity of dissipation rate as a whole.

It may be noted that for the parameterization of *Dis* in eqn (11), the condition of non-zero level of energy loss by waves is involved for frequencies of the order of peak frequency, σ_p or lower, and this reflects the existence of background dissipation processes. This sort of parameterization for *Dis* is introduced in the ModWAM model.

3. Area of study and data used for the verification

3.1 Area of study

Water depth of the study area is prepared using ETOPO2 (Earth Topography 2 minute) bathymetry obtained from the National Geophysical Data Centre, USA, with a spatial resolution of 1.5° x 1.5°. Sensitivity analysis of the wave model, when we extended the southern boundary of Indian Ocean to 60°S, proved that the inclusion of south Indian Ocean in the model domain significantly improves

the model performance (Samiksha et al., 2012). Hence, we considered the model domain bounded by the latitudes 60°S to 30°N and longitudes 10°E to 144°E (Fig. 1a).

3.2 Data used

We used the moored buoy (network established by the National Institute of Ocean Technology, Chennai) data available with the Indian National Centre for Ocean information Services (INCOIS), Hyderabad for the north Indian Ocean (Arabian Sea and Bay of Bengal) (Fig. 1b) to verify the model results. The quality checks performed on the raw data are given in Tiwari et. al (2009). Wave data were measured at the rate of 1 Hz for 17 minutes at three hours duration. The frequency range between 0.04 and 0.10 Hz was considered for low frequency (swell) components and between 0.10 and 0.50 Hz for high frequency (wind sea) components (Rajesh et al. 2009). But, we have considered the range 0.04 - 0.125 Hz as swell region, and 0.125 - 0.50 Hz as wind sea region in the spectrum. The data availability and data duration of each moored buoy is given in Fig. 2. From these set of buoys, we have chosen 10 buoys with long-term data for comparison with numerical simulation results (Table 1). We used ECMWF's Reanalysis (ERA-Interim) winds as the input to the wind wave model (<http://www.ecmwf.int/research/era/do/get/era-interim>), which are available at 6 hourly interval and 1.5° x 1.5° resolution (now available at 0.75°x0.75° resolution at http://apps.ecmwf.int/datasets/data/interim_full_daily/). The ERA-Interim data was compared with moored buoy data winds, which were referenced to 3m height; but, corrected to 10m height using wind profile power law.

The model significant wave height was also compared with the altimeter wave height data available on the IFREMER CERSAT. The database is developed using the Geophysical Data Records (GDR) for each altimeter, which includes altimeter significant wave heights of 16 years period from the six altimeter missions ERS 1& 2, TOPEX/Poseidon, GEOSAT FollowON (GFO) (Naval Oceanographic Office 2002), Jason-1 (Picot et al. 2003) and ENVISAT (ESA 2002). Various quality flags applied to different altimeter datasets are detailed in Queffeuou et al. (2003, 2004). The extracted altimeter track data were further interpolated and converted into grid (1.5°) data for comparison.

4. Results and discussion

The accuracy of ERA winds was verified against buoy winds at two locations: DS2 in the Arabian Sea (Fig. 3a) and DS5 in the Bay of Bengal (Fig. 3b). Correlation coefficients of 0.9 (bias = 0.38 m/s, rmse = 1.37m/s) and 0.86 (bias = -0.14m/s, rmse = 1.53m/s) were obtained for the wind speeds at DS2 and DS5, respectively. Seasonal variability, including monsoon conditions are clearly seen in the ERA-Interim winds as observed in the buoy measurements. This close match between the re-

analysis data and the measured wind data gives us the confidence to use ERA- Interim winds for the analysis and model simulations. Further, higher resolution winds will definitely enhance the model results. The current results are in agreement with Dee et al. (2011) for long term comparison of ERA- Interim with in-situ wind and wave data.

WAM (cycle 4) and ModWAM models were run for the period 2000- 2006. Trial runs were carried out by varying the three coefficients C_{IN} , C_{DIS} and C_{NL} corresponding to wind input, dissipation and nonlinear source functions, representing the physical parameterization of input and dissipation source terms. Based on the trial runs, 27 independent time-series of continuous measurements (0.5 to 1.5 year duration) data was extracted. We varied the fitting parameters to obtain the most accurate result. The variations ranged as below for each parameter, corresponding to our understanding of their validity:

$$0.9 \cdot 10^4 \leq C_{NL} \leq 1.5 \cdot 10^4, \quad (15.1)$$

$$0.4 \leq C_{IN} \leq 0.6; \quad (15.2)$$

$$0.3 \leq C_{DIS} \leq 0.5; \quad (15.3)$$

and

$$10^{-6} \leq b_L \leq 5 \cdot 10^{-6} \quad ; \quad (15.4)$$

$$10^{-5} \leq \gamma_0 \leq 5 \cdot 10^{-5} \quad ; \quad (15.5)$$

$$10^{-1} \leq \gamma_0 \leq 5 \cdot 10^{-1} \quad ; \quad (15.6)$$

The best accuracy was found when $C_{IN}=0.5$, $C_{DIS}=0.55$ and $C_{NL} =12000$. Also, as stated in eqns. (15.1-and 15.6) two background coefficients corresponding to the input and dissipation source functions were tuned slightly to get the best results. Few results obtained from the combinations of the parameters are explained further in spectral comparison of the measured and modeled output. Significant wave height values, H_s , obtained from the two models, WAM and ModWAM, were compared with measurements of 10 moored buoy and altimeter data in the Indian Ocean for the period 2000-2006. Statistical analysis was carried out in order to ascertain the performance of the models, and we find good improvement in the wave simulation by ModWAM. The error estimates calculated for H_s obtained from WAM and ModWAM are given in Tables 1 and 2.

Considering the wind and wave conditions prevailing over the Indian Ocean during different seasons, southwest and northeast monsoons and extreme weather conditions, we have tuned the input, non-linear and dissipation coefficients till accurate results are obtained. Significant wave heights H_s obtained from the two models are compared with buoy measured H_s (at DS01 location in the Arabian Sea) and altimeter H_s , and presented in Fig.4 (a) & (b). The comparison shows that ModWAM

reproduced H_s of all seasons better than WAM. When wave heights are relatively small, WAM overestimates and underestimates when high peaks are present, especially during southwest monsoon (June- September). In fact, several simulations that have been made with both the models, and their comparison with moored buoy measurements at several locations (10) proved precisely that ModWAM provides a better presentation for high waves during monsoon season (for example, southwest monsoon during June-September), as shown in the typical figure (Fig. 4). In Fig. 4, though data availability of DS01 buoy is limited (7 months), it can be noted that the ModWAM reproduced the high waves (significant wave heights of the order of 6.0 m during the southwest monsoon season) more accurately than the WAM; but, still there is underestimation of H_s during high wave conditions. The RMSE of WAM and RMSE of ModWAM in Table 1 indicate the improvement in ModWAM results compared to WAM. We do not find any difference in the RMSE (Table 2) between ModWAM and Altimeter H_s statistics (as compared to ModWAM and buoy H_s in Table 1). As land contamination is present in the altimeter data (very close to the coast), we should consider this altimeter data with caution. The altimeter H_s have been used along with model results, only to complement the comparison of model results with buoy data, and not for validation of model results. Hence, we have chosen those altimeter values, which were closer to the buoy locations.

We observe in Fig. 4 that the ModWAM reproduced the wave conditions at DS01 location well, except for higher peaks (extreme weather events). In order to ascertain model performance for extreme weather events, we considered one cyclone case, which occurred off Goa in May 2001. Simulations were carried out for this event by varying the three source function coefficients, and the results are presented in Fig. 5. We find that when we set the model with low coefficients for all three source functions, the model underestimates the wave heights. When we increased both C_{DIS} and C_{IN} simultaneously (but < 1.0), there was not much change in wave heights, and when both the coefficients were increased further (>1.0), it was observed that there was abnormal increase in wave heights, even beyond the range of measured data. When the simulation was carried out with values less than 1 for C_{IN} and C_{DIS} and by varying the nonlinear coefficient C_{NL} , we find that the model results approach very closer to the measurements during the cyclone peak as well as before and after the cyclone (Fig. 5). Additionally, it may be noted that NL -mechanism is proportional to the 6th power of wave steepness, ϵ . For this reason, the rate of nonlinear energy transfer through the spectrum is proportional to ϵ^4 , i.e. it is a very slow mechanism. Moreover, NL term is responsible for increasing the wave length during wind wave evolution, permitting waves to grow to larger heights, but maintaining small value of wave steepness, ϵ (Polnikov 2002, 2003).

For the study of wave characteristics at a particular location, spectral description of sea state is very important. In the present study, we wanted to examine the match between ModWAM and measured wave spectra off Goa, at 25 m water depth, especially in the case of double-peaked spectra. Fig. 6 shows the comparison of modeled spectra of all cases with measured spectra. The high frequency peak is not brought out in the model output. Along the coast of India, in general, about 60% of the wave spectra observed are multi-peaked; when H_s is more than 2 m, measured wave spectra are mainly single peaked. The double peaked spectra are mainly swell dominated with average value of the difference between peak frequencies around 0.09 Hz (Kumar, 2003). The multi-peaked spectrum plotted in Fig. 6 is pertaining to shallow water (depth = 25m). We find that windsea is missing in the model spectrum, but swell peak in the model spectrum matches very well with the measured spectrum. It has been noted that in certain versions of WAM, an artificial feature is present which prevents windsea growth in the presence of long swell (see Bidlot et al. 2007), in particular in coastal areas. It has to do with how the high frequency tail is imposed after each source term integration. Therefore, the present model underestimates spectral energy at high frequencies (irrespective of single or multi-peaked). This problem in the model code will be rectified in future.

We calculated difference between the energies of modeled and measured spectra over the entire frequency range at 3 hourly intervals for all cases, both for multi-peaked spectra (Fig. 7) and select single-peaked spectra (Fig. 8). When C_{DIS} was reduced or C_{IN} was increased, there was overestimation in the model results, especially, in the low frequency region (case II). Case III is the combination, when $C_{IN} = 0.55$ and $C_{DIS} = 0.5$. In order to check the effect of C_{NL} term, various numerical experiments were carried out. It was observed that higher values of C_{NL} underestimate the model results in the high frequency range. Case IV represents the best results obtained from the combination of coefficients of all the three source functions. We can also observe from Figs. 7 and 8 that the model behavior in the low frequency band (0.0740 - 0.0985 Hz) is similar for all cases, irrespective of single or multi-peaked spectra (average overestimation in the band is approximately $0.4 \text{ m}^2/\text{s}$). However, the error is less in single peaked spectra than in the multi-peaked spectra. Further improvements are required in ModWAM for the accurate prediction of multi-peaked spectra.

5. Conclusions

WAM (cycle 4) and ModWAM models were run by varying the three coefficients C_{IN} , C_{DIS} and C_{NL} , corresponding to wind input, dissipation and nonlinear source functions, representing the physical parameterization of input and dissipation source terms. WAM (Cycle 4) was used as it is with no more tuning. ModWAM results show that there is improvement in wave height prediction

over WAM (cycle 4). One case study was carried out for an extreme weather event to assess the performance of ModWAM, and we find that ModWAM results are more accurate compared to earlier version, especially for the cyclone peak time. Comparison of wave spectra shows that ModWAM still underestimates energy in the high frequency region and overestimates energy in the low frequency region, and this discrepancy primarily arises when spectra are multi-peaked. When the spectrum is single-peaked, the model reproduces the waves accurately, and the spectrum matches with the measured spectrum, but, not so, when the spectrum is multi-peaked.

Acknowledgements

We thank Directors of National Institute of Oceanography (CSIR-NIO), Goa, India and IAPRAS, Russia for their support and interest in this study. The first author acknowledges the Dept. of Science & Technology (DST), India for supporting her research work through Women Scientist Scheme (WOS-A). We are grateful to ECMWF for providing the required ERA wind data and INCOIS, Hyderabad for providing the buoy data for model validation. We are also thankful to *CERSAT*, *IFREMER*, *France* for providing the required altimeter data. The NIO contribution number is xxxx.

References

- Abdalla S., Bidlot, J., Janssen P., 2005. Assimilation of ERS and ENVISAT wave data at ECMWF, ENVISAT & ERS Symposium, Salzburg, Austria, 6-10 Sep. 2004 (ESA SP-572, Apr. 2005).
- Aboobacker, V.M., Vethamony, P., Sudheesh, K., Rupali, S.P., 2009. Spectral characteristics of the nearshore waves off Paradip, India during monsoon and extreme events. *Nat. Hazards* 49, 311–323.
- Aboobacker, V.M., Vethamony, P., Rashmi, R., 2011a. “Shamal” swells in the Arabian Sea and their influence along the west coast of India. *Geophys. Res. Lett.* 38, L03608. doi:10.1029/2010GL045736.
- Aboobacker V. M., R. Rashmi, P. Vethamony and H. B. Menon, 2011b. On the dominance of preexisting swells over wind seas along the west coast of India. *Cont. Shelf Res.* 31, 1701-1712. doi:10.1016/j.csr.2011.07.010.
- Aboobacker V. M., P. Vethamony, Samiksha S. V., Rashmi R., and Jyoti, K., 2013. Wave transformation and attenuation along the west coast of India: Measurements and numerical simulations. *Coastal Engineering Journal* Vol. 55, No. 1, pp.1350001 (21 pages).
- Ardhuin, F., T. H. C. Herbers, G. P. van Vledder, K. P. Watts, R. Jensen, and H. C. Grabber, 2007. Swell and slanting-fetch effects on wind wave growth. *J. Phys. Oceanogr.* 37, 908–931.
- Ardhuin, F., Rogers, E., Babanin, A. V., Filipot, J. F., Magne, R., Roland, A., van der Westhuysen, A., Queffelec, P., Lefevre, J. M., Aouf, L., and Collard, F., 2010. Semi-empirical dissipation source functions for ocean waves. Part I: Definition, calibration, and validation. *J. Phys. Oceanogr.* 40, 1917–1941.

Babanin, A.V., I.R. Young, and M.L. Banner, 2001. Breaking probabilities for dominant surface waves on water of finite constant depth. *J. Geophys. Res.* 106(C6), 11659-11676

Babanin, A.V., 2011. *Breaking and Dissipation of Ocean Surface Waves*. Book, Cambridge University Press, 480p

Banner, M. L., Gemmrich, J. R., and Farmer, D. M., 2002. Multiscale measurements of ocean wave breaking probability. *J. Phys. Oceanogr.* 32, 3364–3375.

Banner, M. L. and Morison, R. P., 2010. Refined source terms in wind wave models with explicit wave breaking prediction. Part I: Model framework and validation against field data, *Ocean Model.* 33, 177–189.

Bidlot, J., P. Janssen, and S. Abdalla, 2007. A revised formulation of ocean wave dissipation and its model impact, Tech. Rep. Memo. 509, ECMWF, Reading, U. K.

Booij, N. , Ris, R. C. and Holthuijsen, L. H. , 1999. A Third Generation Wave Model for Coastal Regions. Part 1. Model Description and Validation. *J. Geophys. Res.* 104, 7649–7666.

Cavaleri, L., J.-H.G.M. Alves, F. Ardhuin, A. Babanin, M. Banner, K. Belibassakis, M. Benoit, M. Donelan, J. Groeneweg, T.H.C. Herbers, and others (The WISE group). 2007. Wave modelling: The state of the art. *Progress in Oceanography* 75, 603–674.

Chalikov, Dmitry, Alexander V. Babanin, 2012. Simulation of Wave Breaking in One-Dimensional Spectral Environment. *J. Phys. Oceanogr.* 42, 1745–1761. doi: <http://dx.doi.org/10.1175/JPO-D-11-0128.1>

Chu, P.C., Cheng K.F., 2008. South China Sea wave characteristics during Typhoon Muifa passage in winter 2004. *Journal of Oceanography* 64, 1-21.

Dee, Dick P., Uppala, Sakari, Simmons, Adrian J., Berrisford, Paul., Poli, Paul., Kobayashi, Shinya., Andrae, U., Balsameda, M A., Balsamo, G., Bauer, P., Bechtold, P., Beljaars, A C M., van de Berg, L., Bidlot, J., Bormann, N., Delsol, C., Dragani, R., Fuentes, Manuel., Geer, A J., Haimberger, Leopold., Healy, S B., Hersbach, Hans., Hólm, E V., Isaksen, L., Kållberg, Per., Köhler, M., Matricardi, M., McNally, A P., Monge-Sanz, B M., Morcrette, J-J., Park, B-K., Peubey, C., de Rosnay, P., Tavolato, C., Thépaut, J-N., Vitart, F, 2011. The ERA-Interim reanalysis: configuration and performance of the data assimilation system. *Quarterly Journal of the Royal Meteorological Society*, 137(656), 553-597.

Donelan, M. A., J. Hamilton, and W. H. Hui, 1985. Directional spectra of wind-generated waves. *Philos. Trans. Roy. Soc. London* 315A, 509–562.

Dungey, J.C., Hui, W.H., 1979. Nonlinear energy transfer in a narrow gravity-wave spectrum. *Proceedings Royal Society London A* 368, 239–265.

Galchenko, A., A.V. Babanin, D. Chalikov, I.R. Young, and B.K. Haus, 2012. Influence of wind forcing on modulation and breaking of deep-water groups. *J. Phys. Oceanogr.* 42, 928-939

Gorman, R., 2003. The treatment of discontinuities in computing the nonlinear energy transfer for finite-depth gravity wave spectra. *Journal of Atmospheric and Oceanic Technology* 20 (1), 206–216.

- Gunther, H., Hasselmann, S. and Janssen, P.A.E.M. 1992. The WAM model cycle 4 ñ Technical Report No. 4. Modellberatungsgruppe, Hamburg.
- Hasselmann, K., 1962. On the non-linear energy transfer in a gravity-wave spectrum. Part 1. General theory. *Journal of Fluid Mechanics* 12, 481–500.
- Hasselmann, K., 1963a. On the non-linear energy transfer in a gravity-wave spectrum. Part 2. Conservation theorems; wave-particle analogy; irreversibility. *Journal of Fluid Mechanics* 15, 273–281.
- Hasselmann, K., 1963b. On the non-linear energy transfer in a gravity-wave spectrum. Part 3. Evaluation of energy flux and swell–sea interaction for a Neumann spectrum. *Journal of Fluid Mechanics* 15, 385–398.
- Hasselmann, K., Barnett, T.P., Bouws, E., Carlson, H., Cartwright, D.E., Enke, K., Ewing, J.I., Gienapp, H., Hasselmann, D.E., Kruseman, P., Meerburg, A., Müller, P., Olbers, D.J., Richter, K., Sell, W., Walden, H., 1973. Measurements of wind–wave growth and swell decay during the Joint North Sea Wave Project (JONSWAP). *Deutsche Hydrographische Zeitschrift A* 8 (12), 1–95.
- Herterich, K., Hasselmann, K., 1980. A similarity relation for the non-linear energy transfer in a finite-depth gravity-wave spectrum. *Journal of Fluid Mechanics* 97, 215–224.
- Hwang, P.A., Wang, D.W., 2004. An empirical investigation of source term balance of small scale surface waves. *Geophysical Research Letters* 31, L15301. doi:10.1029/2004GL020080.
- Janssen, P., 2004. *The Interaction of Ocean Waves and Wind*. Cambridge University Press, 300 pp.
- Janssen, P. A. E. M., K. Hasselmann, S. Hasselmann, G. J. Komen, H. Gunther, and L. Zambresky, 1994. Numerical modelling of wave evolution. *Dynamics and Modeling of Ocean Waves*. G. J. Komen et al., Eds., Cambridge University Press, 205–257.
- Kahma, K. K., and C. J. Calkoen, 1994. Growth curve observations. *Dynamics and Modeling of Ocean Waves*, G. J. Komen et al., Eds., Cambridge University Press, 174–182.
- Komen, G. J., K. Hasselmann, and S. Hasselmann, 1984. On the existence of a fully developed wind-sea spectrum. *J. Phys. Oceanogr.*, 14, 1271–1285.
- Komen, G.J., Cavaleri, L., Donelan, M., Hasselmann, K., Hasselmann, S., Janssen, P.A.E.M. 1994. *Dynamics and Modelling of Ocean Waves*. Cambridge University Press, Cambridge, 532 pp.
- Kumar, V.S., Anand, N.M., Kumar, K.A., Mandal, S., 2003. Multipeakedness and groupiness of shallow water waves along Indian coast. *Journal of Coastal Research* 19, 1052-1065.
- Kukulka, T. and Hara, T., 2005. Momentum flux budget analysis of wind-driven air-water interfaces. *J. Geophys. Res.* 110, C12020, doi:10.1029/2004JC002844.
- Lavrenov, I.V., 2001. Effect of wind wave parameter fluctuation on the non-linear spectrum evolution. *Journal of Physical Oceanography* 31, 861–873.
- Lavrenov, I.V., 2003. Numerical study of non-stationary solution of Hasselmann equation. *Journal of Physical Oceanography* 33, 499–511.

- Lionello, P., Günther H., Janssen P.A.E.M., 1992. Assimilation of altimeter data in a global third generation wave model. *Journal of Geophysical Research* 97 (C9), 14453-14474.
- Manasseh, R., Babanin, A.V., Forbes, C., Rickards, K., Bobevski, I., Ooi, A., 2006. Passive acoustic determination of wave-breaking events and their severity across the spectrum. *Journal of Atmospheric and Oceanic Technology* 23 (4), 599–618.
- Miles, J.W., 1957. On the Generation of Surface Waves by Shear Flows. *Journal of Fluid Mechanics* 3, pp. 185-204.
- Phillips, O. M., 1977. *The Dynamics of the Upper Ocean*. 2nd ed. Cambridge University Press, 366 pp.
- Phillips, O. M., 1985. Spectral and statistical properties of the equilibrium range in wind-generated gravity waves. *J. Fluid Mech.* 156, 505–531.
- Polnikov, V.G., 1993. On a description of a wind–wave energy dissipation function. In: Donelan, M.A., Hui, W.H., Plant, W.J. (Eds.), *The Air–sea Interface. Radio and Acoustic Sensing, Turbulence and Wave Dynamics*. Rosenstiel School of Marine and Atmospheric Science, University of Miami, Miami, FL, pp. 277–282.
- Polnikov, V. G. and L. Farina, 2002. On the Problem of Optimal Approximation of the Four-Wave Kinetic Integral. *Nonlinear Processes in Geophysics* 9 (5/6), 497–512.
- Polnikov, V. G., 2003. The Choice of Optimal Discrete Interaction Approximation to the Kinetic Integral for Ocean Waves. *Nonlin. Proc. Geophys.* 10 (6), 425–434.
- Polnikov, V. G., 2005. Model for Wind Waves with an Optimized Source Function. *Izv. Akad. Nauk, Fiz. Atmos. Okeana*, 41 (5), 655–672
- Polnikov V.G., Dymov ,V.I., Pasechnik T.A., Lavrenov, I. V., Abuzyarov, Z. K. and S. A. Sannasiraj, 2008. Testing and verification of the wind wave model with an optimized source function. *Oceanology*. v. 48, no. 1, p. 11-18.
- Polnikov V.G., 2010. Wind-Wave Model with an Optimized Source Function. *Izvestiya, Atmospheric and Oceanic Physics* 41, No. 5, 2005, pp. 594–610.
- Polnikov V.G., 2012a. Spectral Description of the Dissipation Mechanism for Wind Waves. Eddy Viscosity Model. *Marine Science* 2(3): 13-26 DOI: 0.5923/j.ms.20120203.01
- Polnikov V.G., Samiksha S.V., Rashmi R., Pogarskii F., 2012b Sudheesh K., Vethamony P., 2012b. Modification of Wind-Wave model WAM and its verification against Buoy data in the Indian Ocean, *Hydro* 2012, IIT Bombay, Mumbai
- Rashmi R., V. M. Aboobacker, P. Vethamony, and M. P. John., 2013. Co-existence of wind seas and swells along the west coast of India during non-monsoon season. *Ocean Science*, 9, 281-292.
- Romero, L., and W. K. Melville, (2010). Numerical modeling of fetch-limited waves in the Gulf of Tehuantepec. *J. Phys. Oceanogr.*, 40, 466–486.
- Samiksha S. V, P. Vethamony, V.M. Aboobacker and R Rashmi, 2012. Propagation of Atlantic Ocean swells in the north Indian Ocean: a case study. *Nat. Haz. Ear. Sys. Sci.* 12, 3605-3615.

- The WAMDI Group. 1988. The WAM—A Third Generation Ocean Wave Prediction Model. *J. Phys. Oceanogr.* 12, 1775–1810
- Tiwari, S., Venkat Sheshu R., Pattabhi Rama Rao E., Udaya Bhaskar T.V.S. and Kirankumar N., 2009. Automated real time quality control system for moored buoy data. INCOIS, Tech. Report, INCOIS-DMG-TR-01-2009 .
- Tolman, H.L., Balasubramaniyan, B., Burroughs, L.D., Chalikov, D.V., Chao, Y.Y., Chen, H.S., Gerald, V.M., 2002. Development and implementation of wind generated ocean surface wave models at NCEP. *Weather and Forecasting* 17, 311–333.
- Tolman, H. L., Banner, Michael L., Kaihatu, James M., 2012. The NOPP operational wave model improvement project. *Ocean Modelling*, 70, 2-10. DOI: 10.1016/j.ocemod.2012.11.011
- Tolman, H. L., 2013. A Generalized Multiple Discrete Interaction Approximation for resonant four-wave nonlinear interactions in wind wave models with arbitrary depth. *Ocean Modelling*, 70, 11-24.
- Vethamony, P., Aboobacker, V.M., Sudheesh, K., Babu, M.T., Ashok Kumar, K., 2009. Demarcation of inland vessels' limit off Mormugao Port region, India: a pilot study for the safety for inland vessels using wave modelling. *Nat. Hazards* 49, 411–420.
- Vethamony, P., Aboobacker, V.M., Menon, H.B., Ashok Kumar, K., Cavaleri, L., 2011. Superimposition of wind seas on pre-existing swells off Goa coast. *Journal of Marine Systems* 87(1): 47-54.
- Violante-Carvalho, N., Ocampo-Torres, F.J. and Robinson, I.S. 2004, Buoy observations of the influence of swell on wind waves in the open ocean. *Applied Ocean Research* 26, pp. 49–60.
- Webb, D.J., 1978. Nonlinear transfer between sea waves. *Deep-Sea Research* 25, 279–298.
- WMO, 1988, *Guide to Wave Analysis and Forecasting*. Secretariat of the World Meteorological Organization, Geneva, Switzerland.
- Yan L., 1987. An improved wind input source term for third generation ocean wave modelling. Scientific report WR-87-8. KNML, The Netherlands, 27 p.
- Young, I.R., Babanin, A.V., 2006. Spectral distribution of energy dissipation of wind-generated waves due to dominant wave breaking, *Journal of Physical Oceanography* 36 (3), 376–394.
- Zakharov, V., 1968. Stability of periodic waves of finite amplitude on the surface of a deep fluid. *Journal of Applied Mechanics* 4, 86–94.
- Zakharov, V.E., Pushkarev, A.N., 1999. Diffusion model of interacting gravity waves on the surface of a deep fluid. *Nonlinear Processes in Geophysics* 6, 1–10.

Table Captions

Table 1. Error Estimates of H_s obtained from WAM and ModWAM (model and buoy)

Table 2. Error Estimates of H_s obtained from WAM and ModWAM (model and altimeter)

Figures Captions

Fig. 1. Model domain (a) and location of moored buoys deployed in the Indian Ocean (b)

Fig. 2. Moored buoy data available in the Indian Ocean

Fig. 3. Comparison of ERA winds (blue line) with buoy winds (black line) at two locations: (a) DS2 (Arabian Sea) and (b) DS5 (Bay of Bengal)

Fig. 4. Scatter plots of (a) buoy measured H_s with WAM and ModWAM and (b) altimeter H_s with WAM and ModWAM at DS01 (1 Jan - 26 July 2005).

Fig. 5. Comparison of model H_s with DS01 buoy and altimeter significant wave heights during May 2001 (cases refer to different values of source function coefficients (C_{IN} , C_{DIS} and C_{NL}); Case II: $C_{in}=0.6$, $C_{dis}=0.55$, $C_{nl}=20000$; Case III: $C_{in}=0.7$, $C_{dis}=0.55$, $C_{nl}=20000$; Case IV: $C_{in}=1.0$, $C_{dis}=0.55$, $C_{nl}=20000$).

Fig. 6. Comparison between measured and modeled 1D wave spectra (single-peaked (13 May 2005; 12:00h) and Multi-peaked (20 May 2005; 12:00h)) off Goa during May 2005; cases refer to different values of source function coefficients (C_{IN} , C_{DIS} and C_{NL}); Case I: $C_{in}=0.65$, $C_{dis}=0.55$, $C_{nl}=10000$; Case II: $C_{in}=0.5$, $C_{dis}=0.4$, $C_{nl}=10000$; Case III: $C_{in}=0.5$, $C_{dis}=0.55$, $C_{nl}=12000$; Case IV: $C_{in}=0.65$, $C_{dis}=0.55$, $C_{nl}=12000$

Fig. 7. Error estimate of measured and modelled wave energy spectra (3h interval on 16 May 2005) over the entire frequency range for multipeaked spectra; Case I: $C_{in}=0.65$, $C_{dis}=0.55$, $C_{nl}=10000$; Case II: $C_{in}=0.5$, $C_{dis}=0.4$, $C_{nl}=10000$; Case III: $C_{in}=0.5$, $C_{dis}=0.55$, $C_{nl}=12000$; Case IV: $C_{in}=0.65$, $C_{dis}=0.55$, $C_{nl}=12000$

Fig. 8. Error estimate of measured and modelled wave energy spectra at select timings over the entire frequency range for singlepeaked spectra

Table 1. Error estimates of H_s obtained from WAM and ModWAM (model and buoy)

Year	Buoy ID	Number of collocations	WAM & buoy				ModWAM & buoy			
			Bias (m)	RMSE (m)	Scatt. Index	Corr .Coe ff	Bias (m)	RMSE (m)	Scatt. Index	Corr. Coeff
2000	DS01	2473	0.12	0.33	0.21	0.97	0	0.22	0.14	0.98
	DS02	2538	0.33	0.4	0.28	0.96	0.2	0.32	0.22	0.97
	SW02	1729	-0.01	0.86	0.54	0.54	0.07	0.6	0.37	0.83
2001	DS01	2531	0	0.46	0.27	0.95	-0.08	0.39	0.23	0.95
	DS02	2772	0.31	0.41	0.3	0.95	0.15	0.29	0.21	0.97
2003	DS03	2887	0.1	0.33	0.2	0.9	-0.09	0.3	0.18	0.93
	DS07	1766	0.04	0.33	0.17	0.9	-0.01	0.22	0.12	0.95
	MB12	2863	0.03	0.35	0.21	0.93	-0.13	0.31	0.19	0.95
2004	DS01	2208	0	0.44	0.25	0.96	-0.08	0.36	0.2	0.96
	DS04	1819	0.05	0.32	0.21	0.93	-0.1	0.28	0.18	0.94
	MB01	2068	-0.05	0.41	0.21	0.97	-0.02	0.29	0.15	0.97
	MB12	2884	0.06	0.36	0.23	0.93	-0.08	0.3	0.19	0.95
2005	DS01	1345	-0.05	0.47	0.28	0.96	-0.15	0.28	0.17	0.98
	DS02	1629	0.19	0.47	0.34	0.91	0.02	0.42	0.3	0.91
	DS04	1421	0.02	0.28	0.20	0.90	-0.14	0.26	0.18	0.95
	OB03	2519	0.26	0.51	0.35	0.91	0.15	0.36	0.25	0.94
2006	DS05	2652	0.32	0.9	0.62	0.18	0.12	0.91	0.63	0.25

Table 2. Error estimates of H_s obtained from WAM and ModWAM (model and altimeter)

Year	Buoy ID	Number of collocations	WAM & Altimeter				ModWAM & Altimeter			
			Bias (m)	RMSE (m)	Scatt. Index	Corr. Coeff	Bias (m)	RMSE (m)	Scatt. Index	Corr. Coeff
2001	DS01	365	0.11	0.41	0.24	0.94	0.01	0.41	0.25	0.94
	DS02	365	0.2	0.41	0.27	0.89	0.04	0.38	0.25	0.91
2003	DS03	345	0.04	0.74	0.44	0.45	-0.12	0.70	0.42	0.56
	DS07	345	0.09	0.33	0.23	0.86	-0.01	0.33	0.23	0.89
	MB12	345	0.20	0.54	0.37	0.79	0.04	0.53	0.37	0.80
2004	DS01	340	0.12	0.34	0.23	0.94	-0.02	0.34	0.22	0.94
	DS04	340	0.16	0.39	0.30	0.85	-0.04	0.36	0.27	0.85
	MB01	340	0.12	0.37	0.26	0.93	0.02	0.37	0.26	0.94
	MB12	340	0.22	0.43	0.33	0.86	0.06	0.41	0.31	0.85
2005	DS01	365	0.07	0.48	0.28	0.92	0.12	0.45	0.27	0.94
	DS02	365	0.17	0.39	0.25	0.90	0.18	0.42	0.27	0.92
	DS04	365	0.11	0.47	0.31	0.80	0.00	0.47	0.31	0.79
	OB03	365	0.16	0.41	0.26	0.91	0.18	0.41	0.27	0.94
2006	DS05	358	0.14	0.34	0.24	0.86	-0.12	0.32	0.23	0.87

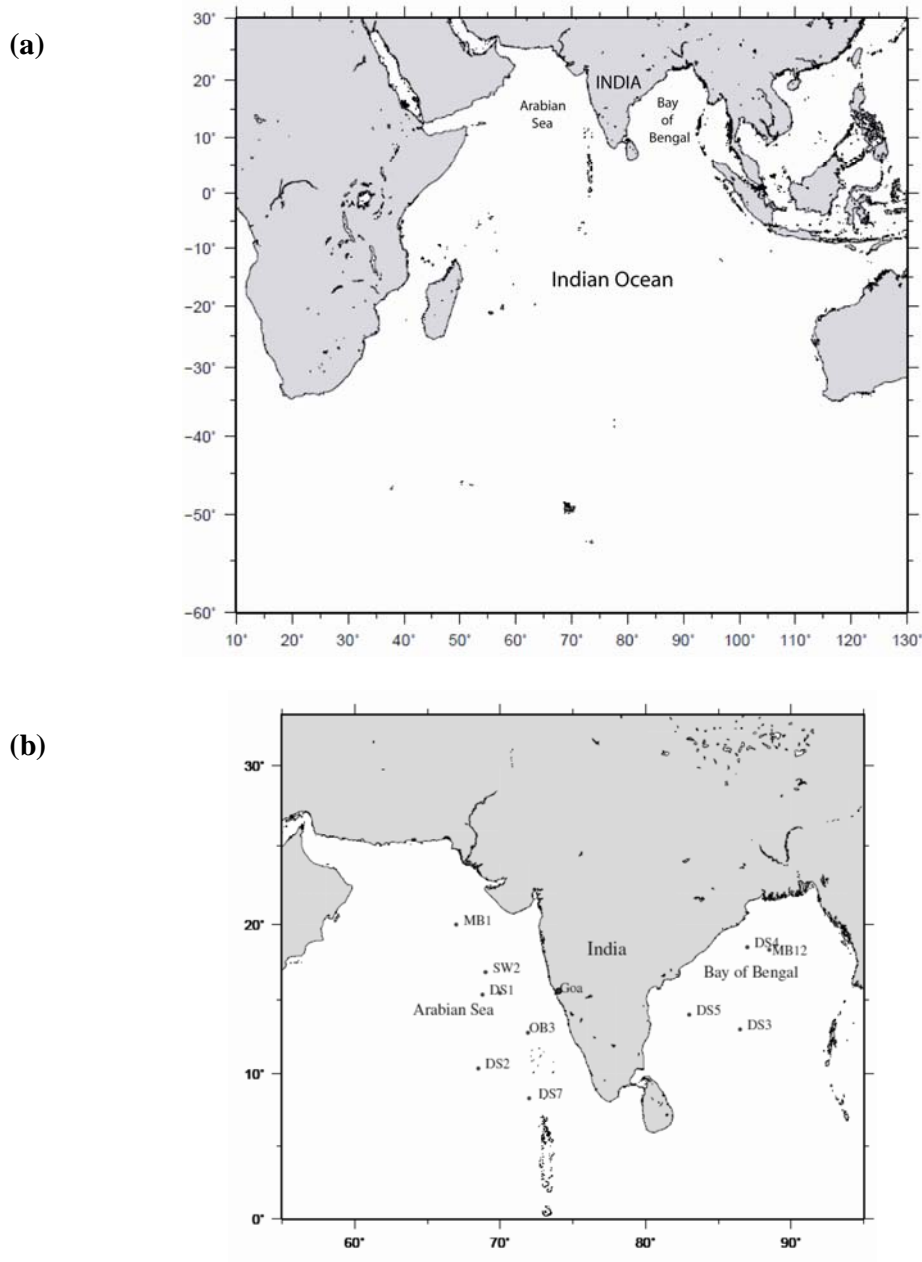


Figure 1. (a) Model domain and (b) location of moored buoys deployed in the Indian Ocean

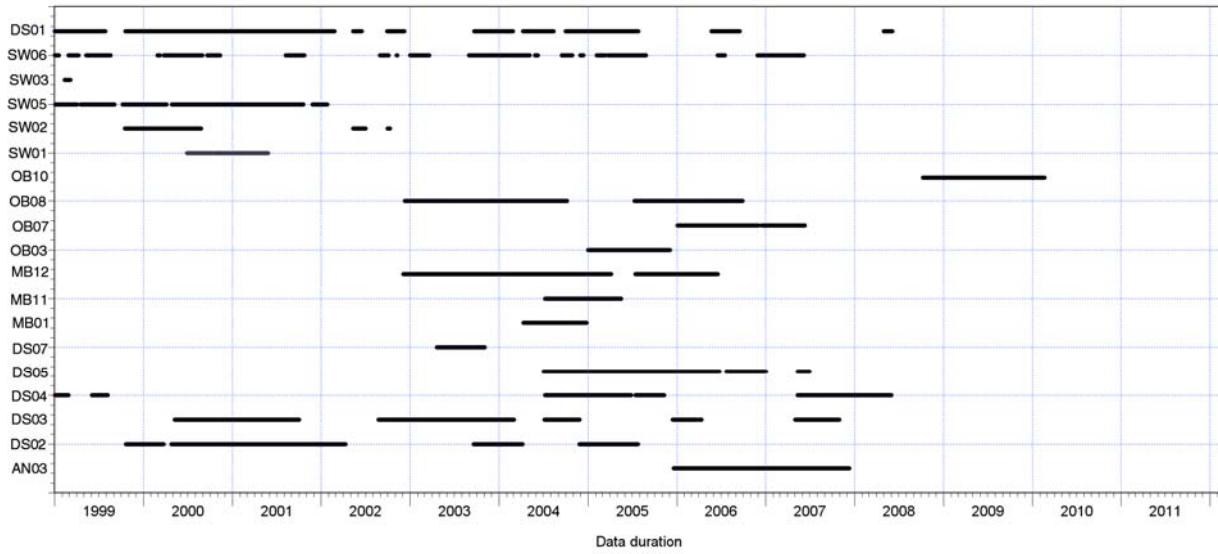
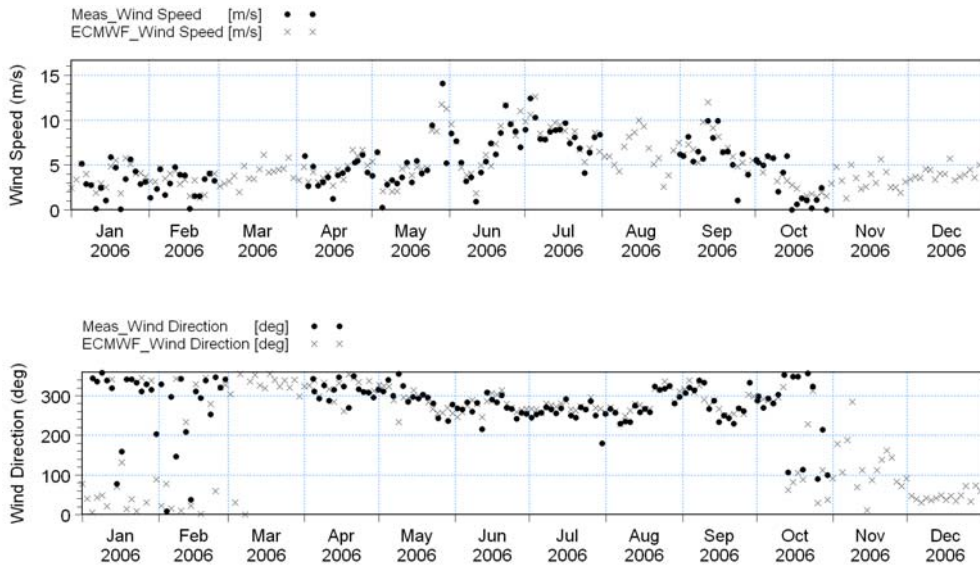
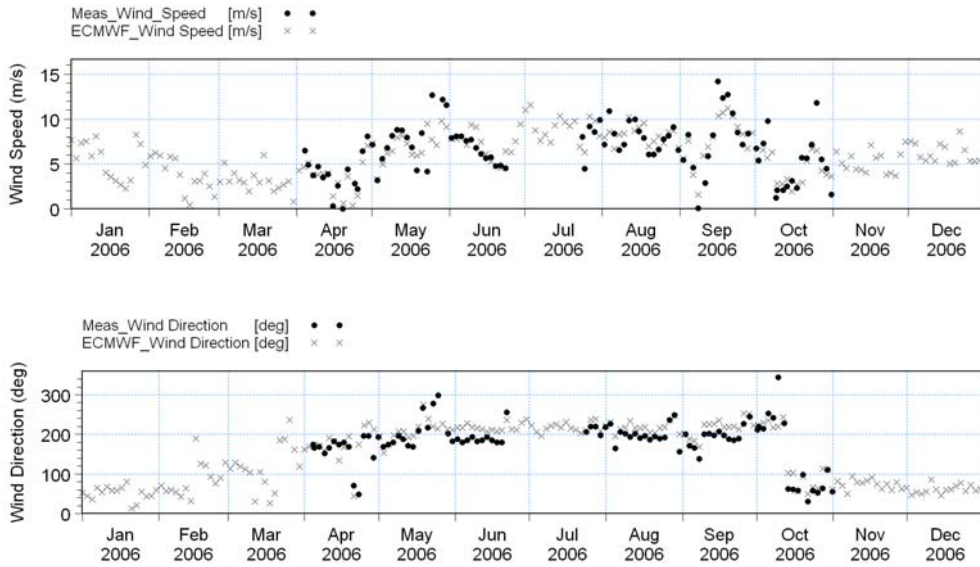


Figure 2. Moored buoy data available in the Indian Ocean



(a)



(b)

Figure 3. Comparison of ERA winds (blue line) with buoy winds (black line) at two locations: (a) DS2 (Arabian Sea) and (b) DS5 (Bay of Bengal)

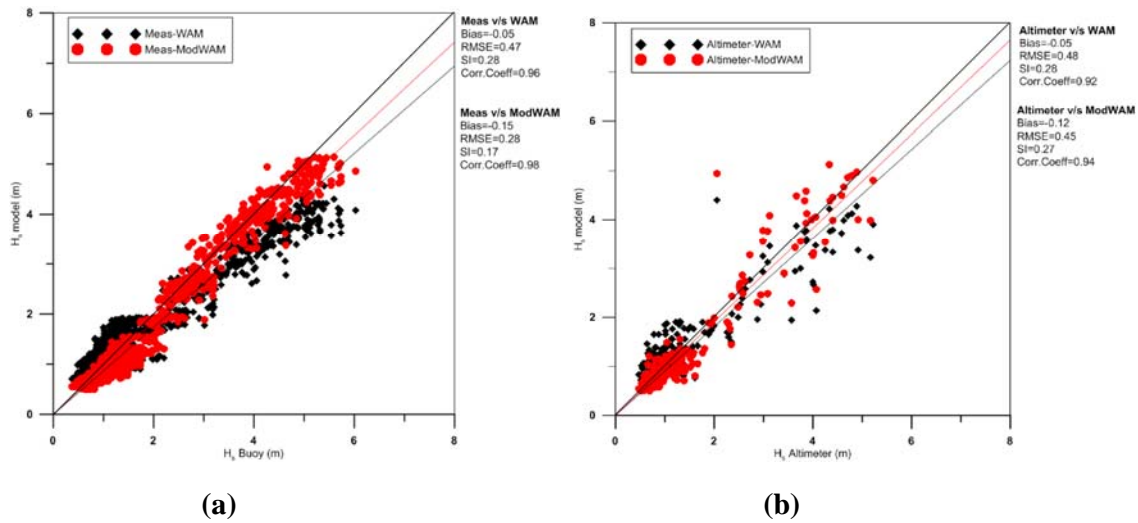


Figure 4. (a) Scatter plot of buoy measured H_s with WAM and ModWAM and (b) Scatter plot of altimeter H_s with WAM and ModWAM at DS01 (1 Jan - 26 July 2005).

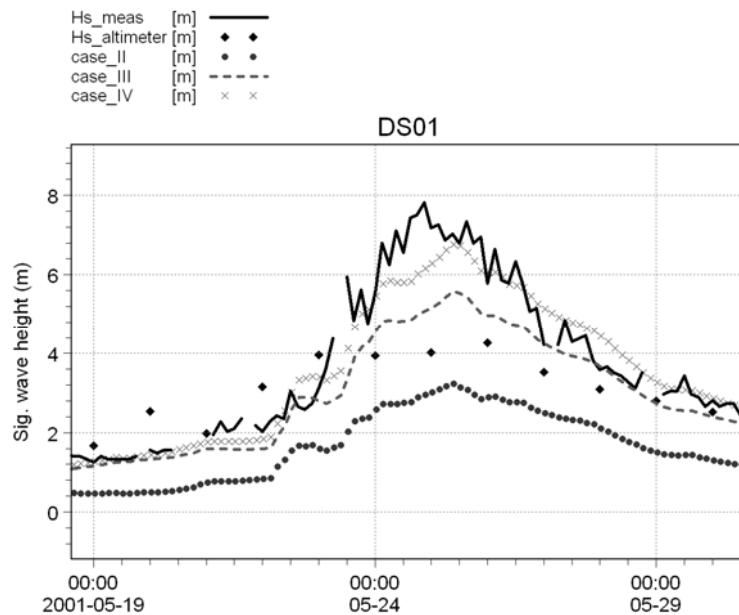


Figure 5. Comparison of model H_s with DS01 buoy and altimeter significant wave heights during a typical cyclone (before, during and after) in 2001 (cases refer to different values of source function coefficients (C_{IN} , C_{DIS} and C_{NL}); Case II: $C_{in}=0.6$, $C_{dis}=0.55$, $C_{nl}=20000$; Case III: $C_{in}=0.7$, $C_{dis}=0.55$, $C_{nl}=20000$; Case IV: $C_{in}=1.0$, $C_{dis}=0.55$, $C_{nl}=20000$).

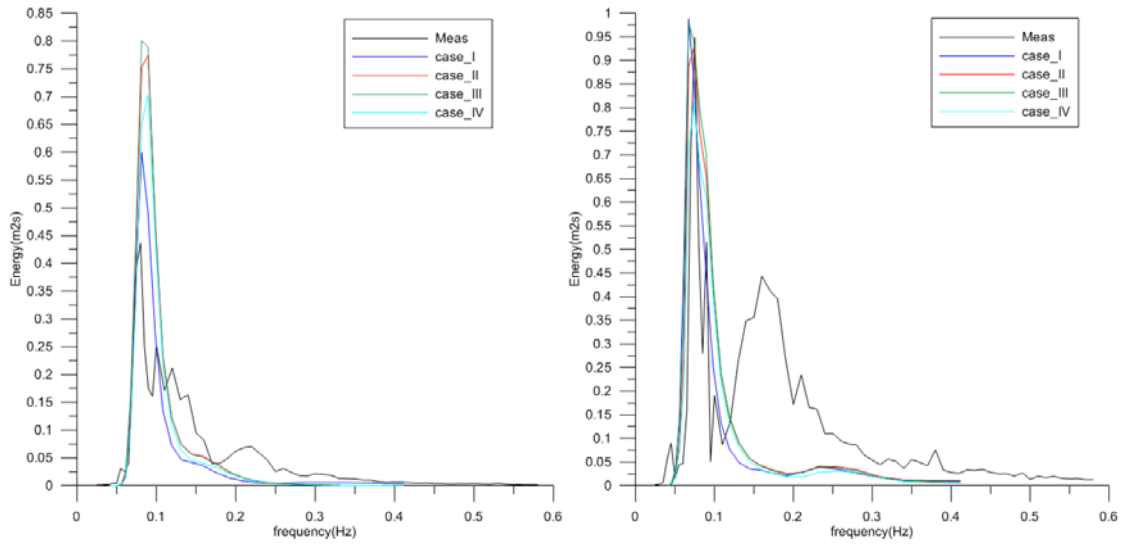


Figure 6. Comparison between measured and modeled 1D wave spectra (single-peaked:13 May 2005; 1200h) and multi-peaked:20 May 2005; 1200h) off Goa during May 2005; cases refer to different values of source function coefficients (C_{IN} , C_{DIS} and C_{NL}); Case I: $C_{in}=0.65$, $C_{dis}=0.55$, $C_{nl}=10000$; Case II: $C_{in}=0.5$, $C_{dis}=0.4$, $C_{nl}=10000$; Case III: $C_{in}=0.5$, $C_{dis}=0.55$, $C_{nl}=12000$; Case IV: $C_{in}=0.65$, $C_{dis}=0.55$, $C_{nl}=12000$

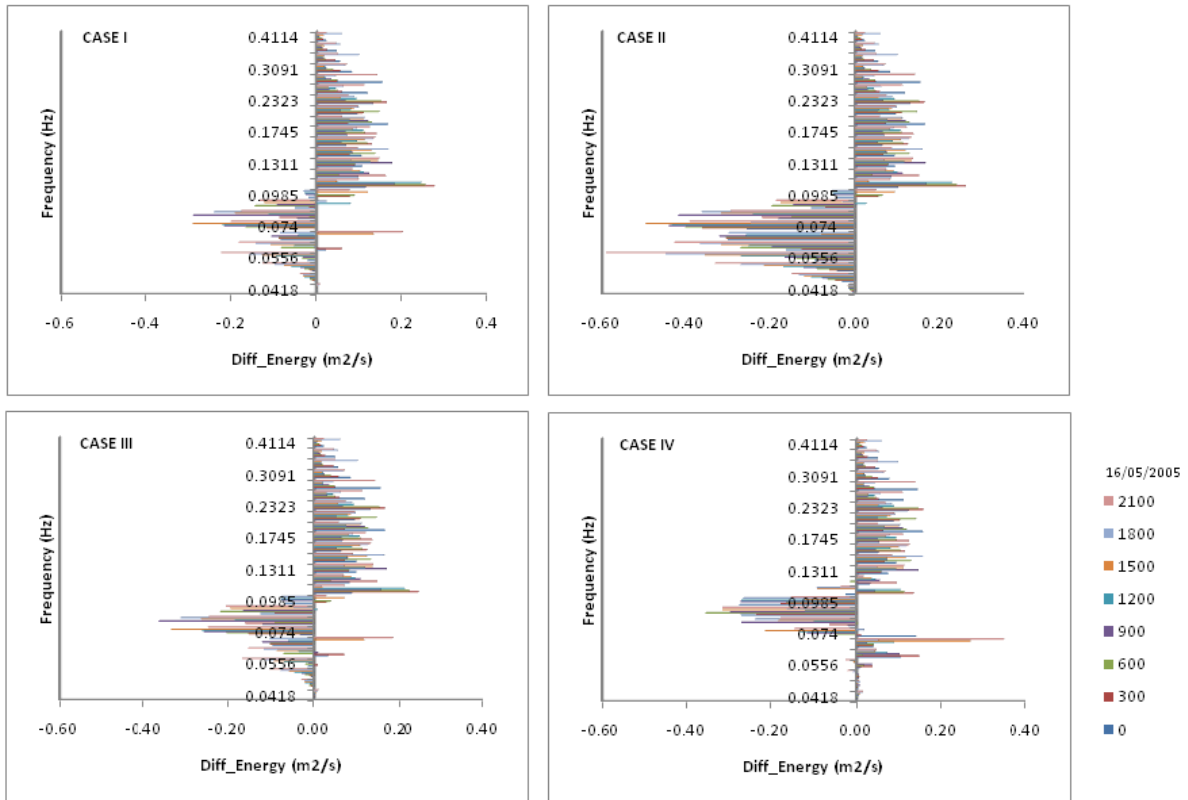


Figure 7. Error estimate of measured and modelled wave energy spectra (3h interval on 16 May 2005) over the entire frequency range for multip peaked spectra Case I: $C_{in}=0.65$, $C_{dis}=0.55$, $C_{nl}=10000$; Case II: $C_{in}=0.5$, $C_{dis}=0.4$, $C_{nl}=10000$; Case III: $C_{in}=0.5$, $C_{dis}=0.55$, $C_{nl}=12000$; Case IV: $C_{in}=0.65$, $C_{dis}=0.55$, $C_{nl}=12000$

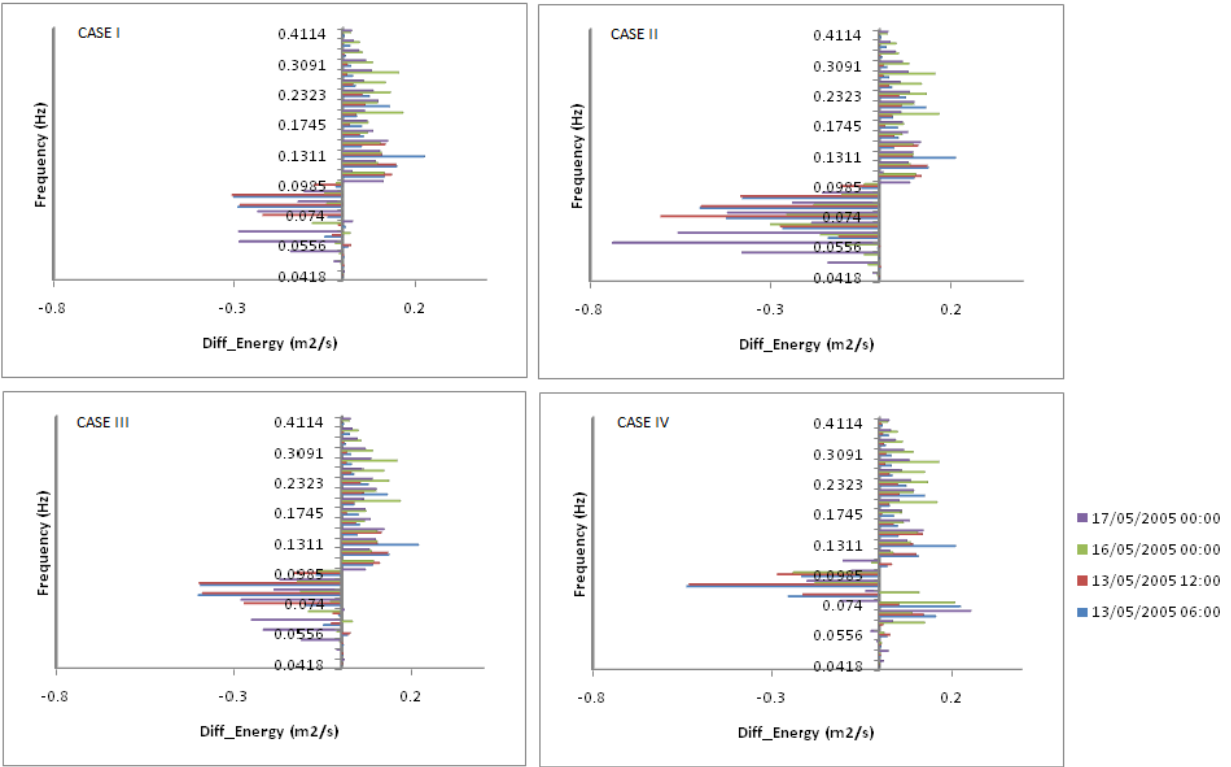


Figure 8. Error estimate of measured and modelled wave energy spectra at select timings over the entire frequency range for singlepeaked spectra